Article

pubs.acs.org/Biomac

Dual MMP7-Proximity-Activated and Folate Receptor-Targeted Nanoparticles for siRNA Delivery

Hongmei Li, Martina Miteva, Kellye C. Kirkbride, Ming J. Cheng, Christopher E. Nelson, Elaine M. Simpson, Mukesh K. Gupta, Craig L. Duvall,* and Todd D. Giorgio*

Department of Biomedical Engineering, Vanderbilt University, 5824 Stevenson Center, Nashville, Tennessee 37235-1631, United States

Supporting Information

ABSTRACT: A dual-targeted siRNA nanocarrier has been synthesized and validated that is selectively activated in environments where there is colocalization of two breast cancer hallmarks, elevated matrix metalloproteinase (MMP) activity and folate receptor overexpression. This siRNA nanocarrier is self-assembled from two polymers containing the same pH-responsive, endosomolytic core-forming block but varying hydrophilic, corona-forming blocks. The corona block of one polymer consists of a 2 kDa PEG attached to a terminal folic acid (FA); the second polymer contains a larger (Y-shaped, 20 kDa) PEG attached to the core block by a proximity-activated targeting (PAT), MMP7-cleavable peptide. In mixed micelle smart polymer nanoparticles (SPNs) formed from the FA- and PAT-based polymers, the proteolytically removable PEG on the PAT polymers shields nonspecific SPN interactions with cells or proteins. When the PAT element is cleaved within an MMP-rich environment, the PEG shielding is removed, exposing the underlying FA and making it accessible for folate receptor-mediated SPN uptake. Characterization of mixed micelles prepared from these two polymers revealed that uptake and siRNA knockdown bioactivity of a 50% FA/50% PAT formulation was dependent on both proteolytic activation and FA receptor engagement. MMP activation and delivery of this formulation to breast cancer cells expressing the FA receptor achieved greater than 50% protein-level knockdown of a model gene with undetectable cytotoxicity. This modular nanoparticle design represents a new paradigm in cell-selective siRNA delivery and allows for stoichiometric tuning of dual-targeting components to achieve superior targeting specificity.

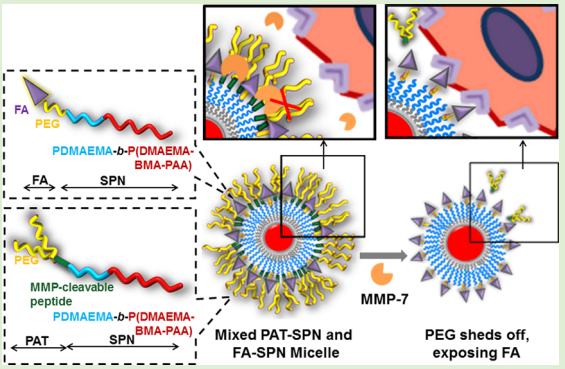

INTRODUCTION

Because of their potent mechanism of action and the ability to design them against otherwise undruggable therapeutic targets, gene-silencing siRNA have been extensively explored for use as a next-generation class of pharmaceutics. A locally administered siRNA therapy entered clinical trials in 2004, and a human trial testing systemic administration of naked siRNA for the treatment of acute renal failure began in 2007.[1] Since then, several siRNA-based approaches have been brought from concept to preliminary clinical testing.[1,2] However, siRNA molecules administered *in vivo* are susceptible to inactivation and rapid renal clearance.[3] As a result, there is currently a strong focus on development of siRNA delivery systems, especially nanocarriers, that improve the pharmacokinetics and enable targeting of siRNA to tumors or other disease sites.

Multifunctional nanoparticles are attractive for cancer therapies due to their potential to be designed to overcome both the extracellular and intracellular delivery hurdles present systemically and in tumors. Nanocarriers are traditionally designed to access tumor tissues via the enhanced permeability and retention (EPR) effect, which results from the leaky vasculature that is characteristic of many tumors.[4] However, the EPR effect alone does not robustly prevent tumor drainage or reverse transport into the systemic circulation;[5,6] as a result, strategies have been sought to improve tumor retention through incorporation of targeting ligands that bind to cell surface receptors,[7,8] moieties that are responsive to biological molecules (i.e., enzymes) secreted in the disease location,[9−11] or "smart" properties that respond to environmental cues (i.e., acidic tumor pH or oxidative stress) to release or activate the therapeutic payload.[12,13]

Functionalization of drug nanocarriers with targeting ligands, such as transferrin and folic acid (FA), has emerged as a mechanism to increase uptake by the targeted cancer cells.[14−16] FA (vitamin B9) is selected for cancer-targeted therapies because folate receptors are rapidly internalized when engaged by FA and because epithelial, ovarian, cervical, breast, lung, kidney, colorectal, and brain cancer cells all abundantly express FA receptor as a mechanism supportive of rapid cell growth.[17] However, some normal tissues, such as the lungs and kidneys,

Received: September 19, 2014
Revised: November 20, 2014
Published: November 21, 2014

also contain cells with high folate receptor expression, increasing the potential for off-target effects.[17] Furthermore, while targeting ligands increase receptor-mediated cell internalization and tumor retention, they do not inherently increase initial tumor accumulation. As a result, targeted vehicles often do not outperform equivalent nontargeted nanoparticles,[18] and there remains to be a significant need to optimize nanocarrier chemicophysical properties for improved stability and extended circulation time.[19]

In order to minimize off-target effects, while also enhancing tumor-specific uptake of siRNA and other chemotherapeutics, a new dual-targeted, pH-responsive siRNA nanocarrier has been developed. This multifunctional smart polymeric nanoparticle (SPN) was designed to concurrently target two key hallmarks of the tumor microenvironment; this new targeting mechanism specifically delivers bioactive siRNA payloads to environments characterized by colocalization of cells with high folate receptor expression[17,20] and elevated matrix metalloproteinases (MMPs), which are overexpressed in many types of highly aggressive and metastatic cancers.[21,22] This design was conceived as an approach to improve selectivity relative to that of conventional targeting approaches by actively delivering payloads only to sites where both of these tumor hallmarks are present. Importantly, this targeting mechanism also incorporates PEGylation for long circulation time, and the resulting SPNs are within a size range optimized for initial EPR-based tumor accumulation *in vivo*.[23,24]

This new targeting approach builds from our previously reported proximity-activated targeting (PAT) SPN containing a cationic dimethlyaminoethyl methacrylate (DMAEMA)-based midlayer for siRNA packaging, as well as an outer PEG layer linked to the corona by a matrix metalloproteinase-7 (MMP7) cleavable peptide.[11] The innermost core of this nanoparticle, like the current design, consisted of a pH-responsive butyl methacrylate (BMA), propyl acrylic acid (PAA), and dimethylaminoethyl methacrylate (DMAEMA) copolymer block that is membrane-disruptive within acidic environments, enabling endosomal escape.[25−27] The previous nanocarrier was functionalized with a 5 kDa proteolytically removable PEG corona; cleavage of this layer shifted the nanoparticle's zeta potential from +6 to +15 mV, resulting in increased cell binding, cell uptake, and gene-silencing activity.[11] However, cellular uptake of this first-generation system was mediated solely by a proteolytically driven increase in zeta potential.

The new targeting strategy disclosed herein was developed to enhance the performance of this promising design and to provide a new, more selective approach to folate receptor targeting. In this approach, MMP activation of the SPN, which has an approximately neutral zeta potential, uncovers underlying FA ligands that are not accessible prior to enzymatic cleavage. Thus, cell surface folate receptors can be engaged only following proteolytic activation within the tumor microenvironment and, at that point, can provide a more robust mechanism of triggering nanoparticle uptake relative to that of sole dependency on increased zeta potential. To achieve this targeting mechanism and to provide better shielding of the underlying cationic layer and improved *in vivo* blood compartment persistence,[28] a 20 kDa Y-shaped PEG block, rather than a 5 kDa PEG, was utilized as the outer corona by linking it through an MMP-cleavable peptide to the underlying poly[(DMAEMA)-*b*-(DMAEMA-*co*-PAA-*co*-BMA)] (pD−pDPB) diblock,[26] yielding PEG_{20k}−peptide−pD−pDPB (referred to as PAT-SPN). The 20k PEG on the PAT-SPN shields folate receptor-mediated SPN uptake in the absence of proteolytic activation by sterically masking a separate, shorter polymer with a 2 kDa PEG block end-functionalized with FA to form FA−PEG_{2k}−pD−pDPB (referred to as FA-SPN). A series of nanoscale mixed micelles comprising different molar ratios of these two polymer constituents (% FA-SPN/% PAT-SPN) was formed and characterized, and an optimized dual-targeted formulation was identified that shows strong potential for improved delivery to breast cancer cells.

MATERIALS AND METHODS

Materials. Chemicals and materials were purchased from Sigma-Aldrich or Fisher Scientific and used as received unless otherwise noted. DMAEMA and BMA monomers were twice passed through a basic alumina column prior to use. 2,2′-Azobis(2-methylpropionitrile) (AIBN) was recrystallized twice using methanol. Dialysis cassettes were purchased from Spectrum. Lipofectamine transfection reagent was purchased from Invitrogen (Carlsbad, CA, USA), and active human MMP7 (MW = 19 kDa) was purchased from EMD Chemicals. PAA monomer was synthesized as previously reported.[29] Maleimide-Y-shape−PEG (20 kDa) (MAL−PEG_{20k}) and heterobifunctional NH_2-PEG-NH-*t*-Boc (2 kDa) were purchased from JenKem Technology USA (Allen, TX, USA).

Synthesis of PEG_{20k}−Peptide (Reversible Addition−Fragmentation Chain Transfer) RAFT Macro Chain Transfer Agent (CTA). The synthesis of 4-cyano-4-(ethylsulfanylthiocarbonyl) sulfanylpentanoic acid (ECT) followed protocols previously described.[26,30] *N*-Hydroxyl succinimide-functionalized-ECT (NHS-ECT) and PEG−peptide macroCTA were synthesized as previously described.[11] Briefly, the MMP7-cleavable peptide (H-VPLSLYSGCG-OH; previously described in ref 11) was synthesized using a PS3 synthesizer (Protein Technologies, Tucson, AZ, USA), purified by HPLC (Waters Breeze system), and confirmed by LC-MS (Waters Synpat ESI-MS). After validation of MMP7 peptide cleavability, 0.21 mmol of peptide and 0.11 mmol of MAL-PEG_{20k} were added to a 50 mL round-bottomed flask and dissolved in 30 mL of anhydrous methanol that had been nitrogen-purged for 30 min. 0.24 mmol of triethylamine (TEA) was then added. The reaction was nitrogen-purged for 30 min and stirred in the dark at room temperature for 24 h. The resulting PEG−peptide conjugate was purified from excess peptide by dialysis against methanol containing 0.2% formic acid, using dialysis tubing of MWCO = 6−8 kDa (Fisher Scientific, Hampton, NH, USA), and the purified product was lyophilized. Purified PEG−peptide conjugate and NHS-ECT were dissolved in a mixture of 50% MeOH/50% DMF and nitrogen purged for 30 min. The reaction was stirred at 30 °C for 48 h and then dialyzed against methanol to remove DMF and excess NHS-ECT. Methanol was subsequently removed by rotary evaporation. Further purification was completed by precipitating the PEG_{20k}−peptide RAFT macroCTA twice from THF into chilled diethyl ether. The ^{1}H NMR spectrum for PEG_{20k}−peptide−ECT is shown in Supporting Information Figure 1.

Synthesis of Folic Acid−PEG RAFT MacroCTA. A FA−PEG RAFT macroCTA was synthesized by modifying a previous protocol.[31] FA (88.3 mg, 0.2 mmol; ^{1}H NMR is shown in Supporting Information Figure 2) and amine-PEG_{2k}-amine-Boc (300 mg, 0.15 mmol; ^{1}H NMR is shown in Supporting Information Figure 3) were co-dissolved in 10 mL of anhydrous DMSO and 5 mL of anhydrous pyridine in a 50 mL round-bottomed flask. The reaction solution was nitrogen-purged for 30 min before the dropwise addition of *N*,*N*′-dicyclohexylcarbodiimide (DCC) (62 mg, 0.3 mmol) dissolved in 1 mL of anhydrous DMSO into the flask. The reaction was stirred in the dark for 48 h and then filtered through a 0.45 mm PTFE membrane filter to remove the precipitate (dicyclohexyl urea). The reaction solution was dialyzed against DMSO to remove excess FA and then dialyzed in methanol. The FA−PEG_{2k} product was isolated by rotary evaporation (^{1}H NMR is shown in Supporting Information Figure 4). The FA−PEG_{2k} product dissolved in 6 mL of trifluoroacetic acid (TFA) was vigorously shaken for 2 h to remove the *t*-Boc protecting group. The resultant FA−PEG_{2k}-NH_2 was purified by precipitation into cold diethyl ether (^{1}H NMR is shown in Supporting Information Figure 5). Purified FA−PEG_{2k}-NH_2 (340 mg, 0.15 mmol) and NHS-ECT (210 mg, 0.58 mmol; ^{1}H NMR is shown in Supporting Information Figure 6) were co-dissolved in a solvent of 33

dx.doi.org/10.1021/bm501394m | *Biomacromolecules* 2015, 16, 192−201

mL of MeOH and 15 mL of DMF and purged with nitrogen for 30 min. The reaction was stirred in the dark at 30 °C for 24 h and then dialyzed against methanol (MWCO = 3000 Da, Fisher Scientific) to remove DMF. Methanol was subsequently removed by rotary evaporation. Further purification was completed by precipitating the FA−PEG_{2k} RAFT macroCTA twice from THF into chilled diethyl ether (^{1}H NMR is shown in Supporting Information Figure 7).

Synthesis of pDMAEMA with PEG_{20k}−Peptide RAFT Macro-CTA or FA−PEG_{2k} RAFT MacroCTA. To synthesize PEG_{20k}−peptide−pDMAEMA (PEG−pep−pD), the RAFT polymerization of DMAEMA with the PEG_{20k}−peptide macroCTA was conducted as previously described.[11] Briefly, PEG_{20k}−peptide macroCTA (234.3 mg, containing 0.0130 mmol CTA content determined by UV−vis absorption extinction coefficient at 320 nm, 8970 mol L^{-1} cm^{-1} in MeOH) was dissolved in 0.57 mL of dioxane in a 2 mL reaction vial under stirring conditions at an initial monomer-to-CTA ratio ($[M]_0/[CTA]_0$) of 150 and CTA-to-initiator molar ratio ($[CTA]_0/[I]_0$) of 6.67. The RAFT polymerization of DMAEMA with PEG_{20k}−peptide macroCTA was conducted at 70 °C under a nitrogen atmosphere. The polymerization was quenched after 3.2 h (27.5% conversion, determined by ^{1}H NMR; characterization of PEG−pep−pD is shown in Supporting Information Table 1). To make FA−PEG_{2k}−pDMAEMA (FA−PEG−pD), DMAEMA, FA−PEG_{2k} macroCTA (82.2 mg, 0.0304 mmol), and initiator were dissolved in 1.37 mL of dioxane in a 5 mL flask under stirring conditions at $[M]_0/[CTA]_0$ of 128 and $[CTA]_0/[I]_0$ ratio of 6.67. The resultant PEG−pep−pD and FA−PEG−pD products were isolated by precipitation into chilled 40:60 v/v diethyl ether/pentane once and by subsequent precipitation into chilled pentane twice. The polymers were redissolved in deionized water and lyophilized.

Synthesis of p(DMAEMA-*co*-PAA-*co*-BMA) Terpolymer Block from PEG−pep−pD MacroCTA or FA−PEG−pD MacroCTA. Synthesis of p(DMAEMA-*co*-PAA-*co*-BMA) terpolymer (pDPB) from PEG−pep−pD was performed as previously described.[11] Briefly, stoichiometric quantities of DMAEMA, PAA, and BMA (25:25:50 mol %), PEG−pep−pD macroCTA (140.0 mg, containing 0.0049 mmol CTA content), and AIBN were dissolved in 1.038 mL cosolvent of 67% dioxane and 33% DMF. The $[M]_0/[CTA]_0$ and $[CTA]_0/[I]_0$ ratios were 360 and 5.56, respectively.

Using the FA−PEG−pD macroCTA, stoichiometric quantities of DMAEMA, PAA, and BMA (23:29:48 mol %), FA−PEG−pD macroCTA (120.0 mg, 0.0080 mmol), and AIBN were dissolved in 1.35 mL cosolvent of 67% dioxane and 33% DMF. The $[M]_0/[CTA]_0$ and $[CTA]_0/[I]_0$ ratios were 430 and 8.33, respectively. The reaction mixture was nitrogen-purged for 20 min and allowed to react at 70 °C for 20 h. Both resultant crude products were precipitated into chilled 50:50 diethyl ether/pentane twice. The resultant polymers, PEG−pep−pD−pDPB and FA−PEG−pD−pDPB were resuspended in pure water, dialyzed against water overnight to remove impurities, and then lyophilized.

Polymer Characterization. Molecular composition of polymer products was determined using ^{1}H NMR spectroscopy (Bruker Biosciences Corporation, Billerica, MA, USA). Absolute molecular weight and polydispersity of the copolymers were characterized by Agilent Infinity gel permeation chromatography (GPC) (Agilent Technologies, Santa Clara, CA, USA) via batch mode by measuring the polymer d*n*/d*c* using known concentrations of each purified polymer sample.

Mixed Micellar Nanoparticle Assembly and Size Measurement by DLS and TEM. Varied ratios of PEG−pep−pD−pDPB (referred to as PAT-SPN) and FA−PEG−pD−pDBP (referred to as FA-SPN) polymers were codissolved in ethanol at a concentration of 20 mg/mL. This solution was then diluted dropwise into a 20-fold volume excess of 1× phosphate buffered saline (PBS) at pH 7.4 under stirring conditions to a final concentration of 1 mg/mL. Micelles were diluted in diH_2O to 0.20 mg/mL for hydrodynamic radius measurement using dynamic light scattering (DLS) (Malvern Zetasizer Nano-ZS). Particle diameter was confirmed using transmission electron microscopy (TEM) imaging using a Philips CM20 system. Carbon film-backed copper grids (Electron Microscopy Sciences, Hatfield, PA, USA) were dipped into 0.15 mg/mL nanoparticle suspension for 1 min and then dipped into 3% uranyl acetate for 15 s. Following each step, grids were gently blotted dried. Grids were dried in a vacuum desiccator overnight prior to imaging.

Assessment of the MMP7 Responsiveness of Mixed Micelles. Proximity activation by MMP7 was determined by GPC and through physicochemical assessments of particle size and surface charge. Micelles in PBS (0.9 mg/mL) were treated with 50 nM active human MMP7 in the presence of 50 μM Zn^{2+} ions (necessary for MMP7 activation) or PBS alone as a control and incubated at 37 °C. Samples were diluted to 0.2 mg/mL with deionized water, and size and ζ-potential were measured on a Malvern Zetasizer Nano-ZS at various time points.

Cell Culture. MDA-MB-231 breast cancer cells (ATCC, Manassas, VA, USA) and MCF-7 mammary tumor cells (ATCC, Manassas, VA, USA) lentivirally transduced to constitutively express firefly luciferase were cultured on standard tissue culture-treated polystyrene in an incubator maintained at 37 °C and 5% CO_2. Cells were maintained in growth media consisting of Dulbecco's modified Eagle's medium (DMEM; Gibco-Life Technology) supplemented with 10% fetal bovine serum (FBS; Gibco) and 50 μg/mL gentamicin (Mediatech, Englewood, CO, USA).

Flow Cytometry and Confocal Microscopy Cell Uptake Measurements. Flow cytometry was used to quantify intracellular delivery of the different mixed micelle formulations. MDA-MB-231 breast cancer cells were seeded at 80 000 cells/mL in a 24-well plate (Corning Costar, Tewksbury, MA, USA) and allowed to adhere overnight. For some samples, micelles were pretreated with 50 nM MMP7 and 50 μM $ZnSO_4$ in the absence of serum for 6 h prior to treatment of cells. In these studies, Alexa488-labeled dsDNA was used as a model for siRNA and was formulated with nanoparticles at a charge ratio of 6:1. Nucleic acid-loaded mixed micelle formulations with or without MMP7 preactivation were then added to the cells at a dsDNA concentration of 50 nM in DMEM supplemented with 10% FBS and 50 μg/mL gentamycin. Free FA in the media at a concentration of 1.1 mg/mL was used for competitive inhibition of folate receptor-mediated nanocarrier internalization. After 6 h of incubation, cells were washed twice with PBS, trypsinized, and resuspended in PBS containing 0.04% trypan blue to quench extracellular fluorescence. Cellular internalization of the micelles was quantified by fluorescence measurements using a BD FACSCalibur flow cytometer (San Jose, CA).

For confocal microscopy experiments, Cy5-labeled dsDNA formulated at a charge ratio of 6:1 were prepared as for the flow cytometry studies. Both MDA-MB-231 and MCF-7 cells were seeded at a density of 80 000 cells/mL in 8-well chamber slides (Nunc/Thermo-Fisher). Cells were treated with PAT-SPN/Cy5-DNA with or without MMP7 preactivation (at 50 nM DNA concentrations) and with or without FA competition for 6 h. After washing twice with PBS and replacing the medium, the live cells were imaged on a Zeiss LSM 510 confocal microscope.

siRNA Protection from RNase Degradation. Ability of micelles to protect siRNA against RNases was measured as previously described[32,33] using the hyperchromic effect, which is the increase in absorbance at 260 nm that occurs when RNA is degraded. Mixed micelles were formulated with siRNA at a charge ratio of 6 and subsequently diluted in 100 μL of dH_2O for a final siRNA concentration of 500 nM. The solution was then placed in a small volume quartz cuvette. 300 nU of Riboshredder RNase blend (Epicenter, Madison, WI, USA) was then added. Absorbance at 260 nm was monitored over 20 min using a Cary 100 UV−vis spectrophotometer (Agilent Technologies, Santa Clara, CA, USA).

Assessment of siRNA Gene Knockdown. MDA-MB-231-Luc cells were seeded at a density of 5×10^4 cells/cm^2 in 96-well plates and allowed to adhere overnight. 50% FA/50% PAT mixed micelle formulations were loaded with luciferase siRNA (Ambion no. AM4629) at a charge ratio of 8. Some samples were preactivated with MMP7 for 6 h and/or free FA was added as a competitive inhibitor, as outlined in uptake studies. Cells were treated for 6 h with mixed micelles at an siRNA concentration of 50 nM. The cells were then given fresh media and incubated for an additional 18 h. To measure luciferase gene silencing, luminescence of each sample was quantified on the Xenogen IVIS-200 (PerkinElmer, Waltham, MA, USA) after adding 0.15 mg/mL

Table 1. Molecular Weight (M_n) and Composition of FA-SPN and PAT-SPN

name	total Mn (kDa)	M_w/M_n	PEG (kDa)	FA or peptide (kDa)	pD (kDa)	pDPB (kDa)	pD (mol % in pDPB)	pB (mol % in pDPB)	pP (mol % in pDPB)
FA-SPN	38.5	1.28	2.0	0.5	13	23.0	21	46	33
PAT-SPN	46.1	1.27	20.0	1.0	6.0	19.1	24	54	22

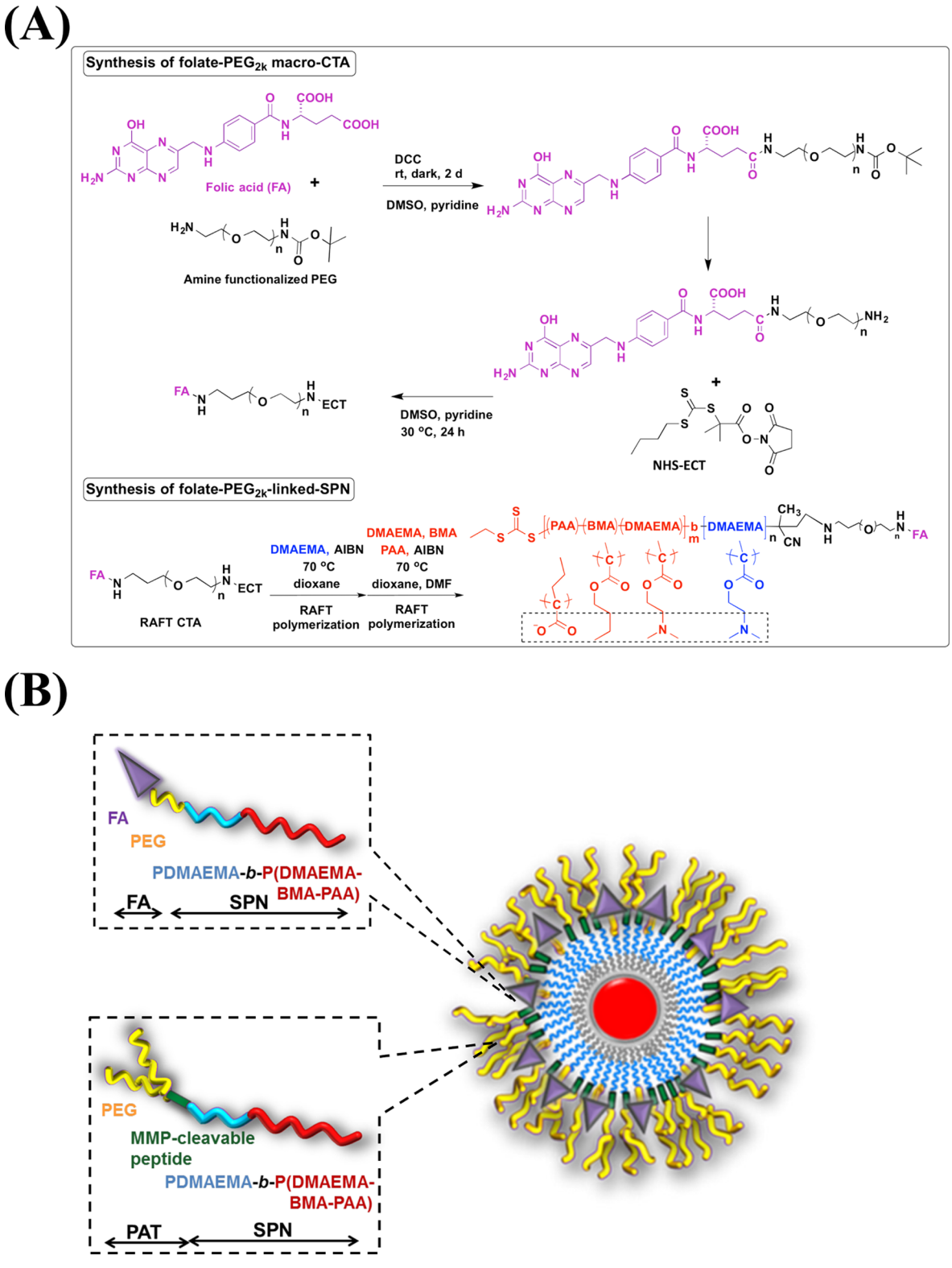

Figure 1. (A) Synthetic scheme of folic acid-modified, 2 kDa PEG-linked diblock copolymer, FA−PEG_{2k}−pD−pDPB (FA-SPN). (B) Schematic of mixed micelle formed from combining FA-SPN and PAT-SPN.

dx.doi.org/10.1021/bm501394m | *Biomacromolecules* 2015, 16, 192−201

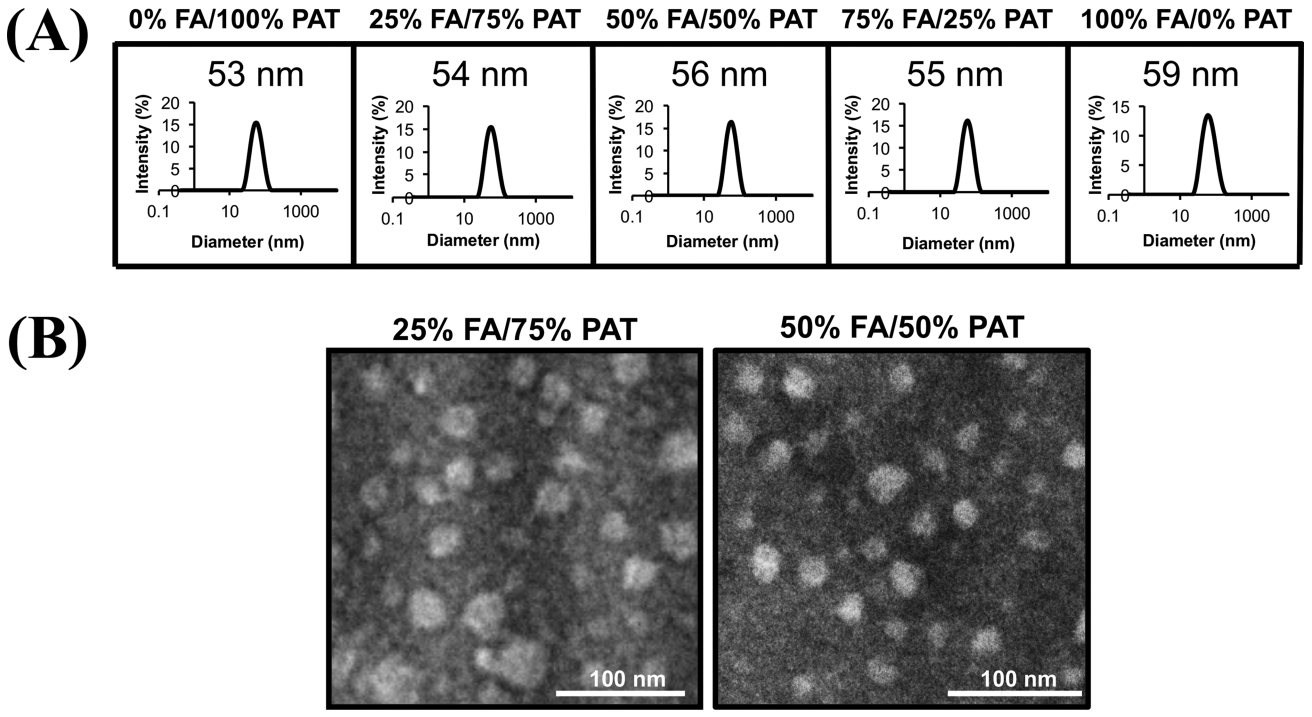

Figure 2. Diameter and morphology of mixed micelle nanoparticles. Self-assembled mixed micelles containing the following percent molar ratios of FA-SPN and PAT-SPN were prepared: 0% FA/100% PAT, 25% FA/75% PAT, 50% FA/50% PAT, 75% FA/25% PAT, and 100% FA/0% PAT. Nanoparticle diameter was determined by DLS in PBS. Shown are representative (A) DLS curves. The lead, dual-targeted mixed micelles (25% FA/75% PAT and 50% FA/50% PAT) were also imaged using (B) TEM, representative images are shown (bottom panels).

luciferin. Luciferase activity was normalized to total protein content measured from the cell lysate of each well using a Bradford assay (Bio-Rad Laboratories Inc., Hercules, CA, USA).

Statistical Analysis. All data are reported as Mean +/− standard error. Analysis of variance (ANOVA) with Tukey's posthoc test was used to establish statistical significance, and $p < 0.05$ was considered to be significant.

RESULTS

Synthesis of PAT-SPN and FA-SPN Polymers. A RAFT polymerization scheme previously reported[11] was used to synthesize a triblock polymer by extending a MMP-cleavable, 20 kDa Y-shaped PEG macroCTA with the RAFT blocks pD−pDPB to form PEG−pep−pD−pDPB (hereafter referred to as PAT-SPN). The total molecular weight of the polymer was 46.1 kDa, with a 6 kDa siRNA-condensing pDMAEMA block and a 19 kDa pDPB block, as determined by NMR and GPC (Table 1). The first-generation PAT-SPN, previously reported, had an outermost corona composed of 5 kDa PEG and possessed a positive (+6 mV) zeta potential.[11] This second-generation PAT-SPN formulation was synthesized with a larger 20 kDa Y-shaped PEG in order to better shield the underlying cationic layer and to limit nonspecific cellular interactions of the particles prior to removal of the MMP-cleavable PAT element.

Using the synthetic scheme in Figure 1A, a new, FA-functionalized triblock FA−PEG−pD−pDPB (hereafter referred to as FA-SPN) polymer was synthesized by RAFT polymerization. A FA−PEG_{2k} macroCTA was synthesized and was subsequently chain-extended through a two-step RAFT polymerization with the pDMAEMA and the p(DMAEMA-*co*-BMA-*co*-PAA) terpolymer blocks. The total molecular weight of the FA−PEG−pD−pDPB polymer was 38.5 kDa, with a 13 kDa siRNA-condensing pDMAEMA block and a 23 kDa p(DMAEMA-*co*-BMA-*co*-PAA) block (Table 1). The shorter 2 kDa PEG was utilized to allow for effective shielding of the FA molecule by the 20 kDa PEG block on the PAT-SPN polymer following co-assembly of the two polymers into mixed micelles. The relatively monodisperse FA-SPN product (PDI = 1.27) was characterized using GPC (Supporting Information Figure 8).

DLS and TEM Size Characterization of Mixed Micelles Containing Both FA-SPN and PAT-SPN Polymers. FA-SPN and PAT-SPN polymers were used to create a series of five mixed micelles that consisted of 0, 25, 50, 75, and 100 mol % FA-SPN, with the remaining fraction composed of PAT-SPN (named based on the mol % FA-SPN followed by the mol % PAT-SPN used to formulate the micelle). The hydrophobic, ampholytic pDPB blocks of both polymers triggers co-assembly of the polymers into micelles following polymer dilution into water (Figure 1B). The size of each mixed micelle composition was characterized by DLS, and the two lead formulations were also imaged using TEM (Figure 2 and Supporting Information Figure 9). All of the micelle compositions had hydrodynamic diameters within the range of 53−59 nm. The TEM images represent the size of the dehydrated micelles, with a partially collapsed corona.[11] These images indicate a consistent size of approximately 30 nm.

Zeta potential and DLS were used to characterize MMP7-dependent changes in the chemicophysical properties of each of the mixed micelles. Prior to MMP7 cleavage, the zeta potential of the mixed micelles inversely correlated to the percent of the 20 kDa PEG-containing PAT-SPN polymer (Figure 3C). Upon exposure to a pathologically relevant concentration of MMP7 (50 nM), all of the mixed micelles containing both FA-SPN and PAT-SPN (at ratios of 25% FA/75% PAT, 50% FA/50% PAT, and 75% FA/25% PAT) exhibited a time-dependent increase in nanoparticle surface charge (Figure 3B) and a decrease in diameter (Figure 3A). The relative decrease in hydrodynamic

dx.doi.org/10.1021/bm501394m | *Biomacromolecules* 2015, 16, 192−201

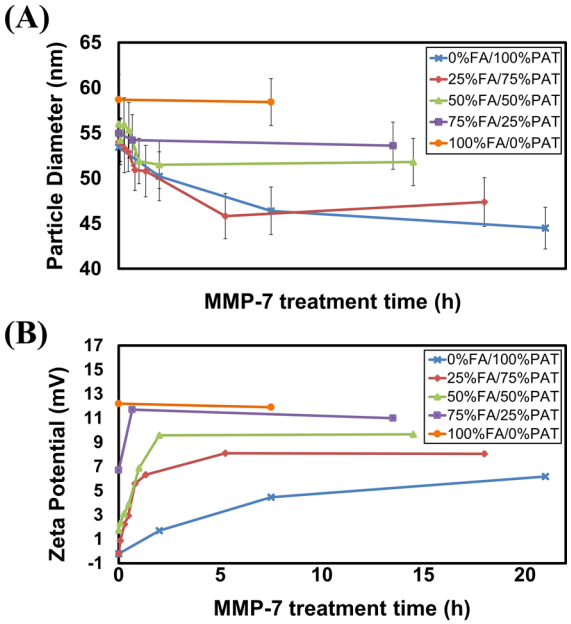

(C)

Micelle composition	Baseline Zeta Potential	Zeta Potential following addition of MMP
0%FA/100%PAT	-0.2 mV	+6.2 mV
25%FA/75%PAT	-0.2 mV	+8.1 mV
50%FA/50%PAT	+1.8 mV	+9.7 mV
75%FA/25%PAT	+6.7 mV	+11.0 mV
100%FA/0%PAT	+12.2 mV	+11.9 mV

Figure 3. Temporal changes in (A) size and (B) zeta potential of mixed micelles following exposure to 50 nM MMP7. (C) Table of baseline and steady-state zeta potential of each nanoparticle formulation following treatment with MMP.

diameter following exposure to MMP7 correlated with the percent of the 20 kDa PEG-containing PAT-SPN polymer in the mixed micelle, consistent with the MMP-activated shedding of the 20 kDa PEG of this polymer accounting for the observed size changes (Figure 3A). As expected, there was no significant change in the diameter or zeta potential of the mixed micelle composed solely of the FA-SPN (100% FA/0% PAT), even after exposure to active MMP7 (58.4 nm, +11.9 mV) for 10 h (Figure 3C). All micelles reached a stable zeta potential over the time course tested, suggesting that maximal peptide cleavage occurs within 10 h of exposure to active MMP7.

MMP7-Triggered and FA-Receptor Enhanced Cellular Uptake in MDA-MB-231 Breast Cancer Cells. The balance of proteolytically activated PAT-SPN and folate receptor-targeting FA-SPN polymers was optimized on the basis of cellular uptake by MDA-MB-231 breast cancer cells, which express high levels of folate receptor (Figure 4A). It was observed that the different mixed micelle formulations caused no significant cytotoxicity within the tested, relevant range of charge ratios (Supporting Information Figure 10). Subsequently, breast cancer cell internalization of mixed micelles at a charge ratio of 6 was measured by flow cytometry with or without proteolytic activation (50 nM of MMP7, a dose that is clinically relevant[34] and was previously shown to reach maximal cleavage of PAT-SPN within 3 h *in vitro*[11]) and in the absence or presence of free FA as a competitive inhibitor. Mixed micelles containing the lowest molar composition of FA-SPN (0% FA/100% PAT, 25% FA/75% PAT, 50% FA/50% PAT) exhibited the least cell internalization in the absence of proteolytic activation (Figure 4A). In contrast, the mixed micelles containing higher percentages of FA-SPN (75% FA/25% PAT and 100% FA/0% PAT) produced significant uptake in the absence of proteolytic activation (5.2× and 7.0× increase compared to that of 0% FA, respectively), reflecting the higher zeta potential, lower PEG density, and higher surface density of exposed FA (statistical comparisons shown in Supporting Information Table 2).

Pretreatment with MMP7 prior to delivery to the cells significantly ($p < 0.05$) increased uptake for all mixed micelles that contained PAT-SPN compared to uptake of the control micelles that had not been activated by MMP7 (Figure 4A and Supporting Information Table 3). Mixed micelles containing the lowest mol % FA-SPN and the highest mol % composition of PAT-SPN (0% FA/100% PAT, 25% FA/75% PAT, and 50% FA/50% PAT) exhibited the largest increase in cell uptake (3.8×, 3.2×, and 2.2×, respectively), proportional with the mol % of PAT-SPN present in the micelle. In contrast, the mixed micelles containing higher percentages of FA-SPN and lower PAT-SPN (75% FA/25% PAT and 100% FA/0% PAT) had a negligible increase in uptake following MMP7 exposure, consistent with the reduced presence of the MMP7-sensitive peptide in the nanoparticle.

To determine the contribution of folate receptor binding to cellular uptake, the cells were treated with excess FA to competitively inhibit nanoparticle engagement of folate receptors. When competition is introduced in the absence of MMP7 activation (no MMP, with FA; light gray bars), the extent of uptake for the 75% FA/25% PAT and 100% FA/0% PAT mixed micelles significantly decreases (0.4× and 0.5×, respectively; $p < 0.05$; Supporting Information Table 3). In addition, folate receptor competition blocks the enhanced cell uptake observed upon MMP7 activation of the mixed micelles with the exception of the 0% FA/100% PAT mixed micelle. The 0% FA/100% PAT composition does not rely on FA-mediated internalization, so the observed increase in uptake following MMP cleavage for this formulation is dependent only on increased zeta potential due to removal of the PEG layer, as in the first-generation PAT-SPN.[11] Optimized mixed micelles (50% FA/50% PAT formulation) were identified on the basis of their significant dependence on both MMP cleavage and folate receptor engagement (i.e., there was a significant increase in uptake following MMP activation, and this effect could be abrogated by addition of free FA). Cellular uptake and intracellular localization of these optimized formulations was confirmed by confocal microscopy (Figure 4B). The dual-targeting properties of the different FA/PAT-SPN mixed micelles were also confirmed in a second breast cancer cell line, MCF-7 cells (Supporting Information Figure 11 and Tables 4 and 5). Taken together, these data demonstrate that efficient dual-targeting was optimized for 50% FA/50% PAT mixed micelle formulations and that these targeting properties were predictable and could be titrated based on the mol % of the FA-SPN and PAT-SPN polymers present in the micelle.

siRNA Protection by Mixed Micelles. Analogous mixed micelles[35] and MMP-activatable micelles[11] are stable and do not aggregate in serum and protect siRNA against degradation by serum components. In the current study, the ability of the mixed micelles to protect the siRNA payload against nuclease degradation was characterized on the basis of the hyperchromic effect (Figure 5).[32] When Riboshredder RNase mix is added, the free siRNA is fully degraded within 20 min. In contrast, degradation of siRNA formulated into 25% FA/75% PAT and

dx.doi.org/10.1021/bm501394m | *Biomacromolecules* 2015, 16, 192−201

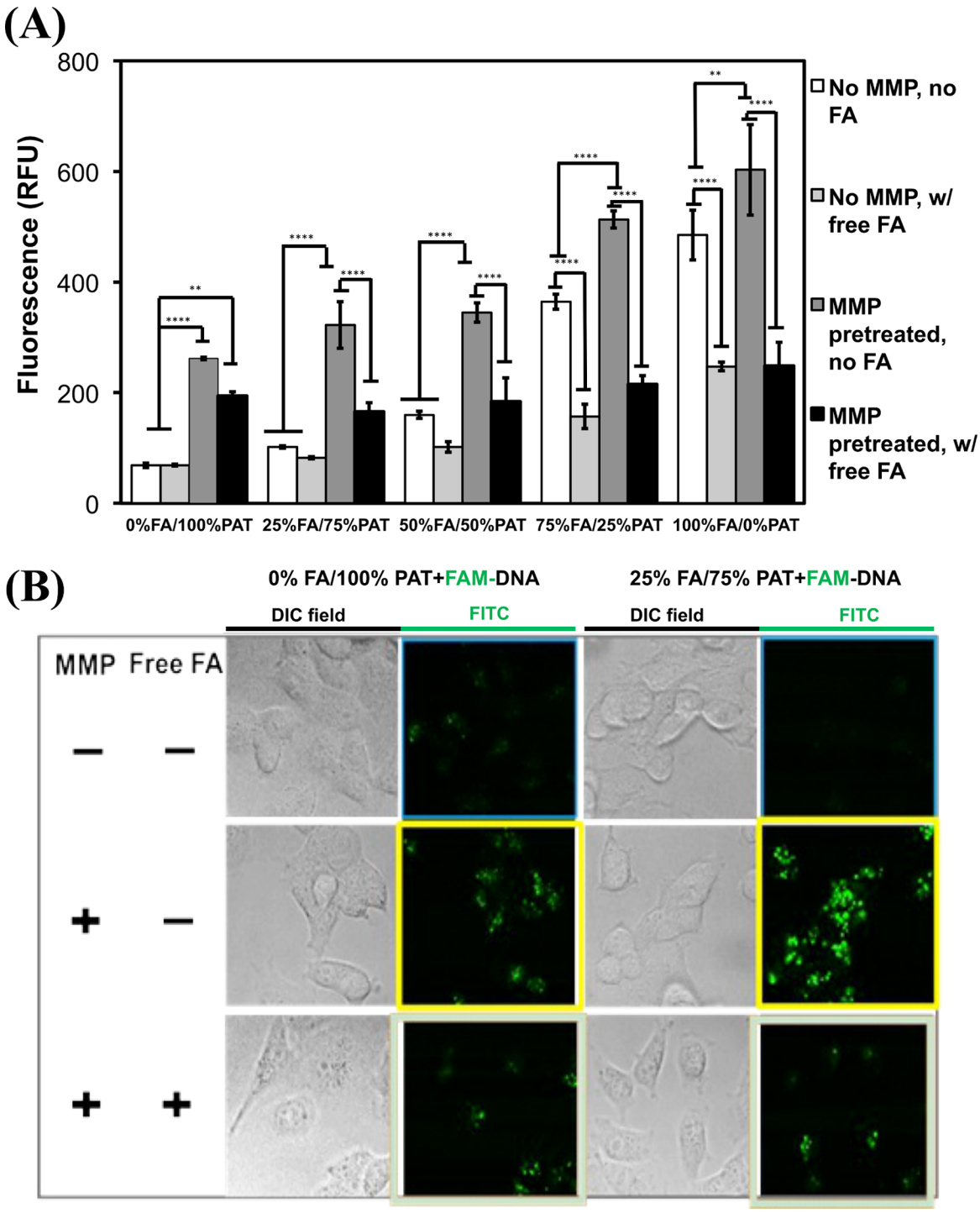

Figure 4. Uptake of optimized (25% FA/75% PAT-SPN and 50% FA/50% PAT-SPN), dual-targeted carriers depends on both MMP7 activation and folate receptor engagement. MDA-MB-231 cells were treated with different FA/PAT-SPN mixed micelle formulations. Internalization was (A) quantified by flow cytometry analysis and (B) observed by confocal microscopy. Treatment with 50 nM MMP7 increased cell internalization of micelle formulations containing the PAT-SPN polymer. Addition of free FA (1.1 mg/mL) to the cell media blocked uptake of the FA polymer-containing mixed micelle formulations. Data are presented as mean ± SEM with $n = 3$. Statistical comparisons can be found in Supporting Information Table 1.

50% FA/50% PAT-SPN micelles was significantly inhibited and reached only about 10% degradation under the same conditions. These data are consistent with previously published results and confirm that surface modifications for dual targeting did not alter SPN nuclease protection.[33]

Gene Knockdown of Model Gene Luciferase *in Vitro*. The extent of functional siRNA delivery using the dual-targeted nanocarrier was assessed *in vitro*. A significant intracellular barrier to siRNA bioactivity is endosomal entrapment; therefore, hemolysis studies were performed to ensure pH-dependent membrane disruptive activity (Supporting Information Figure 12).[36] The varied mixed micelle surface chemistries incorporated by the FA-SPN and PAT-SPN polymers did not alter the previously established pH-dependent membrane disruption behavior of the pDPB core-forming polymer block.[26] To test for siRNA bioactivity, MDA-MB-231 breast cancer cells stably

dx.doi.org/10.1021/bm501394m | *Biomacromolecules* 2015, 16, 192−201

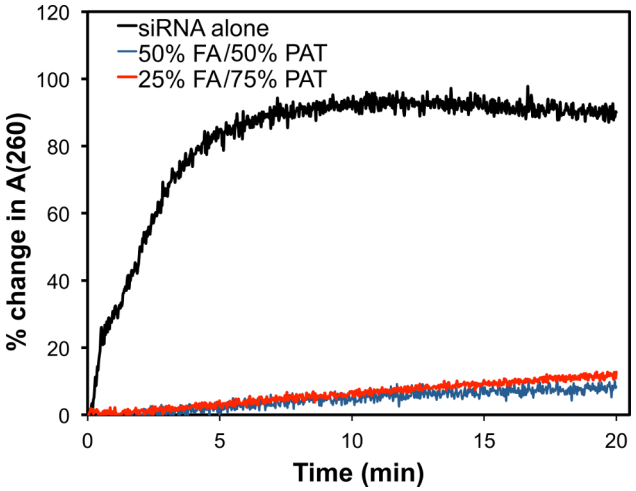

Figure 5. Mixed micelle formulations protect siRNA from degradation. Free siRNA and siRNA loaded into 50% FA/50% PAT-SPNs at an N/P of 6 were subjected to a Riboshredder RNase blend, and degradation was quantified by the hyperchromic effect (percentage increase of absorbance at 260 nm (A_{260})). An increase in A_{260} reflects siRNA degradation.

expressing the model gene firefly luciferase were treated with the 50% FA/50% PAT mixed micelle, as this particle possessed optimal dual MMP7 and folate receptor-dependent internalization (Figure 3). The 50% FA/50% PAT micelles were used to deliver a 50 nM dose of either scrambled or luciferase (Luc)-specific siRNA. There was no significant difference in luciferase activity between nontreated (NT) control cells compared to that of scrambled siRNA-treated cells (Figure 6). However, luciferase expression was significantly decreased (25%) in breast cancer cells treated with Luc siRNA-containing micelles in the absence of MMP7 pretreatment. These data are consistent with our previously published data confirming that MMPs synthesized by cells can, at least partially, activate PAT-SPNs in culture.[11]

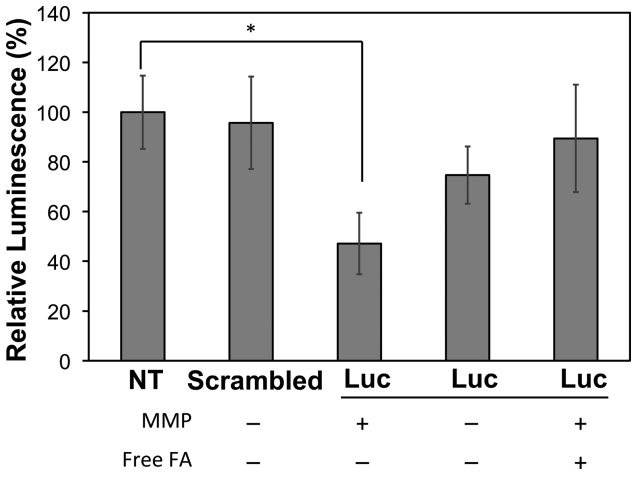

Figure 6. Gene-silencing bioactivity of siRNA delivered by dual-targeting FA/PAT-SPNs is significantly increased by MMP cleavage and FA receptor binding. MDA-MB-231 cells stably expressing luciferase were treated with 50% FA/50% PAT-SPN loaded with luciferase siRNA at a charge ratio of 8. The samples that were exposed to MMP (50 nM) but not free folic acid (1.1 mg/mL) achieved significant silencing of the target gene. Data are presented as the mean ± SEM with $n = 4$. *$p < 0.05$ compared to NT.

Enhanced proteolytic activation of the micelle with exogenous MMP7 prior to delivery to cells increased knockdown of luciferase to 53%. This MMP7 activation-dependent decrease in gene expression was abrogated when excess FA was introduced to the cells 1 h before micelle delivery; this FA-treated group preserved 90% of the luciferase expression, which is not significantly different from that of NT or scrambled siRNA-treated control cells. Taken together, these data further confirm the dual-targeting nature of the 50% FA/50% PAT mixed micelles, as well as their ability to effectively achieve siRNA intracellular bioavailability.

DISCUSSION

Previous studies have demonstrated the utility of FA-functionalized nanoparticles for enhancing siRNA delivery and gene knockdown compared to that of untargeted nanoparticles,[31,37] including in ovarian cancer.[15] However, while folate receptor expression is high in cancer cells, it is also highly expressed in the kidneys and lungs,[17] and *in vivo* studies show undesirably high accumulation of folate-targeted nanoparticles in these tissues.[28,37] One popular mechanism to enhance the pharmacokinetics of cationic particles is the use of PEGylation; however, nanoparticle passivation with PEG also reduces interactions with cells, thereby limiting the cellular uptake in target tissues.[15] The new design examined in this work uses a two-stage delivery strategy to minimize the interaction of nanoparticles with nontarget cells through a PEG corona that is removed only in the proximity of active MMP7 to (1) reveal FA ligands and (2) increase zeta potential for enhanced uptake specifically in target tissues. Such multifunctional approaches are typically challenging to fabricate, purify, and validate, especially if the future goal includes clinical translation. This work seeks to partially overcome practical obstacles of complexity through the use of modular molecular structures that can yield nanoscale vehicles with multiple functions in controllable proportions through the preparation of mixed micelles.

While mixed micelles have been pursued for other applications, this is, to our knowledge, is the first application where mixed micelles have been used to characterize the relative contributions to biological performance from multiple, independent specific targeting components for siRNA delivery. The design, created from two molecular structures containing near-identical core-forming hydrophobic blocks and different hydrophilic corona-forming segments, enables the facile preparation of micelles presenting solely FA-SPN (100% FA/0% PAT), solely PAT (0% FA/100% PAT), or any proportion of these two features. The molecular weights of the polymers used to create the mixed micelles were specifically selected to ensure effective shielding of the FA moieties by the 20 kDa PEG block (Figure 1B). Varying the ratios of PAT-SPN and FA-SPN enables the identification of a nanoparticle composition optimized for *in vivo* delivery (effectively shielded zeta potential) that achieves a high level of specific uptake by cancer cells (where there is colocalized presence of MMP7 activation and FA binding). Additionally, this family of nanoscale siRNA delivery agents, composed of only two molecular species, eases the preparation and characterization of materials. While the most straightforward route to clinical translation may come in the form of MMP-activatable tumor margin diagnostics, dual-targeting of MMP-responsive chemotherapeutic carriers has led to recent improvements in tumor-specific targeting for *in vivo* delivery and has been found to improve chemotherapeutic response.[38] Therefore, the dual-targeting nature of our micelles, as well as the controlled

dx.doi.org/10.1021/bm501394m | *Biomacromolecules* 2015, 16, 192−201

synthesis and ability to rapidly tune and optimize our carrier properties, may represent a breakthrough that will accelerate clinical translation of MMP-targeted RNAi. Thus, this new approach provides manufacturing simplicity and it produces complex nanomaterials with multifunctional advantages to facilitate translation toward clinical applications.

To overcome the lack of cell specificity inherent in many chemotherapeutics, our design relies on enhanced active cellular uptake through the folate receptor, occurring after peptide cleavage in the MMP7-rich tumor microenvironment. Mixed micelles containing PAT-SPN are MMP-responsive (Figure 3) and result in significant increases in breast cancer cell uptake following MMP7 activation and exposure of the FA targeting component (Figure 4). The high level of uptake prior to MMP7 activation achieved by particles containing higher percentages of FA-SPN is undesirable, as it suggests the potential for nonspecific uptake in nontarget cells lacking the MMP7-rich tumor microenvironment (Figure 4). The 50% FA/50% PAT-SPN micelles exhibit a low zeta potential (+1.8 mV), which suggests that the presence of 50% PAT-SPN effectively shields the charge contributed by the pDMAEMA layer utilized for siRNA packaging (i.e., 100% FA/0% PAT-SPN zeta potential is +12.2 mV). Cells expressing folate receptor have limited uptake of the 50% FA/50% PAT-SPN particles in the absence of MMP7, suggesting that this mixed micelle will largely avoid off-target tissues that express folate receptor, a significant limitation of previous approaches using FA targeting. Cellular uptake decreases with FA competition in the presence of MMP7 activation, consistent with the hypothesis that the FA moieties on the nanoparticles serve as an active breast cancer cell uptake mechanism (Figure 4). In summary, 50% FA/50% PAT has been identified as optimal for dual MMP-responsiveness and folate receptor targeting.

By limiting nonspecific cell uptake until the micelle is in the tumor microenvironment, the proposed delivery system establishes a new paradigm for achieving tissue specificity. This is expected to avoid the debilitating side effects caused by current chemotherapies[39] and is anticipated to have especially high impact in the clinical management of distributed disease. An additional consideration of nanoparticle drug delivery for eventual clinical translation is ensuring an optimal size (10−100 nm) for extended circulation in the bloodstream and accumulation at disease sites.[4] All of the dual-targeted mixed micelles compositions tested herein have a consistent hydrodynamic diameter of 53−59 nm and minimal zeta potential (Figure 3), giving them the added advantage of being large enough to reduce renal clearance but small enough to avoid macrophage phagocytic removal.[40] This design also ensures the intracellular release of the payload specifically after uptake by folate receptor-expressing tumor cells and intracellular trafficking to the endosome. Furthermore, the hydrophobic nanocarrier core provides the potential for co-delivery of siRNA and a hydrophobic drug, which is particularly important for delivery of an siRNA that will sensitize multidrug-resistant cancer cells to chemotherapies.[41] On the basis of its optimal dual-targeting cellular uptake characteristics and minimal cytotoxicity, we used the 50% FA/50% PAT-SPN micelles to assess siRNA payload delivery. Our nanoparticles provide significant protection of siRNA, which is otherwise rapidly degraded in an environment that is rich in RNases, overcoming another one of the major obstacles for use of siRNA-based gene therapy to treat cancer.[42] Data presented here confirm that breast cancer cells can be effectively targeted by nanoparticles with a folate receptor-dependent mechanism of cell uptake. Importantly, micelles activated by MMP7 and delivered in the absence of free folate achieved significant (greater than 50%) knockdown of target gene activity (Figure 6). This degree of model gene knockdown is comparable to that of FA-targeted, polyethylenimine (PEI)-based siRNA nanocarriers at the same siRNA concentration (50 nM) that knocked down target gene expression by ∼40%.[43] However, strongly cationic siRNA delivery systems, such as those based on PEI, are generally unsuitable for use *in vivo*, especially by intravascular (IV) administration.

CONCLUSIONS

The combination of near neutral zeta potential, appropriate size, and undetectable cytotoxicity at active doses suggests that the FA/PAT-SPN micelles described in this work are ideal for effective tumor localization following IV injection. These data combined with results supporting that the optimized mixed micelle formulation is active only in environments characterized by the presence of both MMP7 activity and folate receptor-expressing breast cancer cells further support the proposed tumor retention and protein knockdown performance of these novel mixed micelles *in vivo*. Taken together, these data indicate that these nanoparticles are well-suited for translation *in vivo* as a highly tunable, dual-targeted siRNA carrier.

ASSOCIATED CONTENT

Supporting Information

Additional methods, ^{1}H NMR spectra, exampled polymer molecular weight and molar mass dispersity (after H-NMR spectra), GPC confirmation of syntheses, additional TEM images, cytotoxicity, additional intracellular uptake plots, hemolysis, and additional statistics. This material is available free of charge via the Internet at http://pubs.acs.org.

AUTHOR INFORMATION

Corresponding Authors

*(C.L.D.) E-mail: craig.duvall@vanderbilt.edu. Tel.: 1-615-322-3598. Fax: 1-615-343-7919.

*(T.D.G.) E-mail: todd.d.giorgio@vanderbilt.edu. Tel.: 1-615-322-3756.

Notes

The authors declare no competing financial interest.

ACKNOWLEDGMENTS

This research was supported by a grant from the Department of Defense Congressionally Directed Medical Research Program (W81XWH-10-1-0446). DLS, spectrofluorimetry, and TEM were conducted through the use of core facilities of the Vanderbilt Institute of Nanoscale Sciences and Engineering (VINSE). Confocal microscopy was performed in the VUMC Cell Imaging Shared Resource (supported by NIH grant nos. CA68485, DK20593, DK58404, HD15052, DK59637 and EY08126).

REFERENCES

(1) Zhou, Y.; Zhang, C.; Liang, W. *J. Controlled Release* **2014**, 270−281.
(2) Videira, M.; Arranja, A.; Rafael, D.; Gaspar, R. *Nanomedicine* **2014**, *10*, 689−702.
(3) Deng, Y.; Wang, C. C.; Choy, K. W.; Du, Q.; Chen, J.; Wang, Q.; Chung, T. K. H.; Tang, T. *Gene* **2014**, *538*, 217−227.
(4) Maeda, H. *J. Controlled Release* **2012**, *164*, 138−144.
(5) Bertrand, N.; Wu, J.; Xu, X.; Kamaly, N.; Farokhzad, O. C. *Adv. Drug Delivery Rev.* **2013**, 2−25.

(6) Ballarín-González, B.; Ebbesen, M. F.; Howard, K. A. *Cancer Lett.* **2013**, 66−80.
(7) Hu-Lieskovan, S.; Heidel, J. D.; Bartlett, D. W.; Davis, M. E.; Triche, T. J. *Cancer Res.* **2005**, *65*, 8984−8992.
(8) Jiang, G.; Park, K.; Kim, J.; Kim, K. S.; Hahn, S. K. *Mol. Pharmaceutics* **2009**, *6*, 727−737.
(9) Hatakeyama, H.; Akita, H.; Kogure, K.; Oishi, M.; Nagasaki, Y.; Kihira, Y.; Ueno, M.; Kobayashi, H.; Kikuchi, H.; Harashima, H. *Gene Ther.* **2007**, *14*, 68−77.
(10) Chien, M.-P.; Thompson, M. P.; Barback, C. V.; Ku, T.-H.; Hall, D. J.; Gianneschi, N. C. *Adv. Mater.* **2013**, *25*, 3599−3604.
(11) Li, H.; Yu, S. S.; Miteva, M.; Nelson, C. E.; Werfel, T.; Giorgio, T. D.; Duvall, C. L. *Adv. Funct. Mater.* **2013**, *23*, 3040−3052.
(12) Gullotti, E.; Yeo, Y. *Mol. Pharmaceutics* **2009**, *6*, 1041−1051.
(13) Gupta, M. K.; Meyer, T. A.; Nelson, C. E.; Duvall, C. L. *J. Controlled Release* **2012**, *162*, 591−598.
(14) Byrne, J. D.; Betancourt, T.; Brannon-Peppas, L. *Adv. Drug Delivery Rev.* **2008**, *60*, 1615−1626.
(15) Li, T. S. C.; Yawata, T.; Honke, K. *Eur. J. Pharm. Sci.* **2014**, *52*, 48−61.
(16) Davis, M. E.; Zuckerman, J. E.; Choi, C. H. J.; Seligson, D.; Tolcher, A.; Alabi, C. A.; Yen, Y.; Heidel, J. D.; Ribas, A. *Nature* **2010**, *464*, 1067−1070.
(17) Parker, N.; Turk, M. J.; Westrick, E.; Lewis, J. D.; Low, P. S.; Leamon, C. P. *Anal. Biochem.* **2005**, *338*, 284−293.
(18) Bartlett, D. W.; Su, H.; Hildebrandt, I. J.; Weber, W. A.; Davis, M. E. *Proc. Natl. Acad. Sci. U.S.A.* **2007**, *104*, 15549−15554.
(19) Nelson, C. E.; Kintzing, J. R.; Hanna, A.; Shannon, J. M.; Gupta, M. K.; Duvall, C. L. *ACS Nano* **2013**, *7*, 8870−8880.
(20) Vihinen, P.; Ala-aho, R.; Kähäri, V.-M. *Curr. Cancer Drug Targets* **2005**, *5*, 203−220.
(21) Wang, F.; Reierstad, S.; Fishman, D. A. *Cancer Lett.* **2006**, *236*, 292−301.
(22) Shiomi, T.; Okada, Y. *Cancer Metastasis Rev.* **2003**, *22*, 145−152.
(23) Jain, R. K.; Stylianopoulos, T. *Nat. Rev. Clin. Oncol.* **2010**, *7*, 653−664.
(24) Chauhan, V. P.; Stylianopoulos, T.; Martin, J. D.; Popović, Z.; Chen, O.; Kamoun, W. S.; Bawendi, M. G.; Fukumura, D.; Jain, R. K. *Nat. Nanotechnol.* **2012**, *7*, 383−388.
(25) Convertine, A. J.; Diab, C.; Prieve, M.; Paschal, A.; Hoffman, A. S.; Johnson, P. H.; Stayton, P. S. *Biomacromolecules* **2010**, *11*, 2904−2911.
(26) Convertine, A. J.; Benoit, D. S. W.; Duvall, C. L.; Hoffman, A. S.; Stayton, P. S. *J. Controlled Release* **2009**, *133*, 221−229.
(27) Duvall, C. L.; Convertine, A. J.; Benoit, D. S. W.; Hoffman, A. S.; Stayton, P. S. *Mol. Pharmaceutics* **2010**, *7*, 468−476.
(28) Xiao, K.; Li, Y.; Luo, J.; Lee, J. S.; Xiao, W.; Gonik, A. M.; Agarwal, R. G.; Lam, K. S. *Biomaterials* **2011**, *32*, 3435−3446.
(29) Kim, J.; Tirrell, D. A. *Macromolecules* **1999**, *32*, 945−948.
(30) Moad, G.; Chong, Y. K.; Postma, A.; Rizzardo, E.; Thang, S. H. *Polymer.* **2005**, *46*, 8458−8468.
(31) Benoit, D. S. W.; Srinivasan, S.; Shubin, A. D.; Stayton, P. S. *Biomacromolecules* **2011**, *12*, 2708−2714.
(32) Kirkland-York, S.; Zhang, Y.; Smith, A. E.; York, A. W.; Huang, F.; McCormick, C. L. *Biomacromolecules* **2010**, *11*, 1052−1059.
(33) Yu, S. S.; Lau, C. M.; Barham, W. J.; Onishko, H. M.; Nelson, C. E.; Li, H.; Smith, C. A.; Yull, F. E.; Duvall, C. L.; Giorgio, T. D. *Mol. Pharmaceutics* **2013**, *10*, 975−987.
(34) McIntyre, J. O.; Fingleton, B.; Wells, K. S.; Piston, D. W.; Lynch, C. C.; Gautam, S.; Matrisian, L. M. *Biochem. J.* **2004**, *377*, 617−628.
(35) Miteva, M.; Kirkbride, K. C.; Kilchrist, K. V.; Werfel, T. A.; Li, H.; Nelson, C. E.; Gupta, M. K.; Giorgio, T. D.; Duvall, C. L. *Biomaterials* **2015**, *38*, 97−107.
(36) Evans, B. C.; Nelson, C. E.; Yu, S. S.; Beavers, K. R.; Kim, A. J.; Li, H.; Nelson, H. M.; Giorgio, T. D.; Duvall, C. L. *J. Visualized Exp.* **2013**, e50166.
(37) Lee, H.; Lytton-Jean, A. K. R.; Chen, Y.; Love, K. T.; Park, A. I.; Karagiannis, E. D.; Sehgal, A.; Querbes, W.; Zurenko, C. S.; Jayaraman, M.; Peng, C. G.; Charisse, K.; Borodovsky, A.; Manoharan, M.; Donahoe, J. S.; Truelove, J.; Nahrendorf, M.; Langer, R.; Anderson, D. G. *Nat. Nanotechnol.* **2012**, *7*, 389−393.
(38) Crisp, J. L.; Savariar, E. N.; Glasgow, H. L.; Ellies, L. G.; Whitney, M. A.; Tsien, R. Y. *Mol. Cancer Ther.* **2014**, *13*, 1514−1525.
(39) Feng, S.-S.; Chien, S. *Chem. Eng. Sci.* **2003**, *58*, 4087−4114.
(40) Alexis, F.; Pridgen, E.; Molnar, L. K.; Farokhzad, O. C. *Mol. Pharmaceutics* **2008**, *5*, 505−515.
(41) Xiong, X.-B.; Lavasanifar, A. *ACS Nano* **2011**, *5*, 5202−5213.
(42) Soutschek, J.; Akinc, A.; Bramlage, B.; Charisse, K.; Constien, R.; Donoghue, M.; Elbashir, S.; Geick, A.; Hadwiger, P.; Harborth, J.; John, M.; Kesavan, V.; Lavine, G.; Pandey, R. K.; Racie, T.; Rajeev, K. G.; Röhl, I.; Toudjarska, I.; Wang, G.; Wuschko, S.; Bumcrot, D.; Koteliansky, V.; Limmer, S.; Manoharan, M.; Vornlocher, H.-P. *Nature* **2004**, *432*, 173−178.
(43) Dong, D.-W.; Xiang, B.; Gao, W.; Yang, Z.-Z.; Li, J.-Q.; Qi, X.-R. *Biomaterials* **2013**, *34*, 4849−4859.